

# Correlation induced Mott-Peierls instability in $\text{K}_2\text{Cr}_8\text{O}_{16}$

Sooran Kim, Kyoo Kim, and B. I. Min

Department of physics, PCTP, Pohang University of Science and Technology, Pohang, 790-784, Korea

In order to explore the driving mechanism of the concomitant metal-insulator and structural transitions in hollandite  $\text{K}_2\text{Cr}_8\text{O}_{16}$ , electronic structures and phonon properties are investigated by employing the *ab initio* density functional theory (DFT) calculations. We have found the significant difference in the phonon dispersion curves between the DFT and the DFT+ $U$  ( $U$ : Coulomb correlation) calculations. The phonon softening instability exists only in the DFT+ $U$  calculation, which indicates that the Coulomb correlation plays an essential role in the structural transition. The lattice displacements of the softened phonon at X explain the observed lattice distortions properly, suggesting the Peierls nesting vector of  $\mathbf{Q}=\mathbf{X}$  (0, 0, 1/2). This finding is in contrast to the previously suggested Peierls nesting vector of  $\mathbf{Q}=\mathbf{M}$  (1/2, 1/2, -1/2). The combined study of electronic and phonon properties manifests that half-metallic  $\text{K}_2\text{Cr}_8\text{O}_{16}$  undergoes the correlation-assisted Peierls transition, upon cooling, to become a Mott-Peierls ferromagnetic insulator.

PACS numbers:

Strongly correlated transition-metal (TM) oxides show rich phases according to pressure, doping, temperature, and so on.<sup>1</sup> Among those, hollandite-type TM oxides  $A_2M_8O_{16}$  ( $A$ = alkali metal,  $M$ = TM element) have drawn recent attention due to their intriguing quasi-one dimensional column structure made of double  $MO$  chains with corner-shared  $MO_6$  octahedra. Despite the similarity in the crystal structures, these materials have different physical properties depending on the TM element.  $\text{K}_2\text{Cr}_8\text{O}_{16}$  and  $\text{K}_2\text{V}_8\text{O}_{16}$  exhibit the metal-insulator transition (MIT) and the structural transition concomitantly upon cooling.<sup>2,3</sup>  $\text{K}_2\text{Cr}_8\text{O}_{16}$  and  $\text{K}_x\text{Ti}_8\text{O}_{16}$  show magnetic transition from paramagnetic to ferromagnetic (FM) phase, with varying the temperature and the carrier concentration, respectively.<sup>4-6</sup> On the other hand,  $\text{K}_2\text{V}_8\text{O}_{16}$  has a complex ground state containing the charge ordering and the spin-singlet structure.<sup>3,7</sup> The possibility of Tomonaga-Luttinger liquid property has also been suggested in  $\text{K}_2\text{Ru}_8\text{O}_{16}$ .<sup>8</sup>

$\text{K}_2\text{Cr}_8\text{O}_{16}$  of present concern exhibits an interesting phase diagram depending on the temperature (T). It would have nominal mixed-valence state with the average electrons per Cr being 2.25 ( $\text{Cr}^{4+} : \text{Cr}^{3+} = 3:1$ ). At high T,  $\text{K}_2\text{Cr}_8\text{O}_{16}$  is a paramagnetic metal with the body-centered tetragonal crystal structure ( $I4/m$ ).<sup>4,9</sup> Figure 1 presents the crystal structure and the corresponding Brillouin zone. Along the  $c$  axis, the double-chain of edge-shared  $\text{CrO}_6$  octahedra exists. Upon cooling, two phase transitions take place. At first, the magnetic transition occurs at 180K from paramagnetic to FM phase. The observed magnetic moment of the system is  $17.7 \mu_B/8\text{Cr}$ .<sup>4</sup> This magnetic transition is not accompanied with the structural transition, and so this phase is still metallic. Interestingly, the FM phase has half-metallic nature. This feature was explained by the double exchange mechanism arising from the Hund coupling between the fully occupied  $d_{xy}$  orbital and the partially occupied  $d_{xz}$  and  $d_{yz}$  of Cr,<sup>10</sup> as in  $\text{CrO}_2$ .<sup>11</sup>

The second transition is the MIT at 95 K. At this transition, the ferromagnetic property is preserved.<sup>4</sup> To explain this property, an insulator version of the double exchange ferromagnetism was proposed.<sup>13</sup> When the MIT was first observed, the structural transition was not detected,<sup>4</sup> and so the charge ordering<sup>14</sup> and the charge density wave<sup>10</sup> were suggested as the mechanism of the MIT. Later, however, the structural transition coexisting with the MIT was observed,<sup>2</sup> from the body-centered tetragonal to the monoclinic structure ( $P 112_1/a$ ) that has an increased unit cell of  $\sqrt{2} \times \sqrt{2} \times 1$ . Based on this newly discovered structure, it was suggested that the MIT is caused by a Peierls instability in the quasi-one-dimensional column structure made of four coupled Cr-O chains running along the  $c$  direction, leading to the formation of tetramers of Cr ions at low T.<sup>2</sup>

There have been a few electronic band structure studies on  $\text{K}_2\text{Cr}_8\text{O}_{16}$ .<sup>2,10,14</sup> By contrast, there has been no phonon study, which can provide a direct clue to the structural transition. Also, the roles of the Coulomb correlation in the MIT and in stabilizing the ferromagnetic insulator (FI) ground state have not been fully understood yet. In this letter, we have investigated electronic structures and the phonon dispersion curves of  $\text{K}_2\text{Cr}_8\text{O}_{16}$  to explore the mechanism of the MIT and the structural transition. To analyze the effect of on-site Coulomb correlation,  $U$ , we studied the phonon properties both without and with  $U$  in the density functional theory (DFT) calculations. We have found that the phonon softening instability occurs only in the DFT+ $U$ , which indicates that the Coulomb correlation plays an essential role in the structural transition. The displacements of normal mode of softened phonon at X (0, 0, 1/2) are quite consistent with the observed structural distortions occurring at the MIT, which produces the Cr tetramers in the four coupled Cr-O chains and their stripe-type arrangement. Noteworthy is that this softening vector  $\mathbf{Q} = \mathbf{X}$  is different from the previously suggested Peierls nesting vector of  $\mathbf{Q} = (1/2, 1/2, -1/2)$ .<sup>2</sup> We have also found that the formation of Cr tetramers is the main origin of opening

the band gap, not the Cr-Cr dimerization in the double-chain of  $\text{CrO}_6$  octahedra.

For the DFT calculations, we employed the pseudopotential band method implemented in VASP,<sup>16</sup> and for the phonon calculations, we employed PHONOPY code.<sup>17</sup> The force constants for the phonon calculation were obtained from the supercell calculation with small displacements by the Hellmann-Feynman theorem.<sup>18</sup> The generalized gradient approximation (GGA) was used for the exchange-correlation functional. Before carrying out the phonon calculations, we performed the full-relaxation, which adjusts the lattice constant and atomic positions. The initial structural data before the full-relaxation were taken from the experiment.<sup>15</sup>  $U$  value

of 3.0 eV was adopted for the GGA+ $U$  calculations.<sup>2</sup> The energy cut off of 520 eV was used for the number of plane wave bases. The  $\mathbf{k}$ -point samplings are  $(6 \times 6 \times 20)$  for the conventional tetragonal unit cell of the FM metallic phase, and  $(4 \times 4 \times 20)$  for the monoclinic unit cell of the FI phase in the Monkhorst-Pack grid.

The  $(2 \times 2 \times 1)$  supercell is selected for the phonon calculation of the FM metallic phase.

We first carried out the band structure calculations for the FM phase of  $\text{K}_2\text{Cr}_8\text{O}_{16}$  both in the GGA and the GGA+ $U$  schemes. Both schemes produces the metallic phase, more precisely, the half-metallic phase, as is consistent with literature.<sup>4,10</sup> The total magnetic moments are  $17.6 \mu_B/\text{f.u.}$  ( $2.3 \mu_B/\text{Cr}$ ) and  $18.1 \mu_B/\text{f.u.}$  ( $2.6 \mu_B/\text{Cr}$ ) in the GGA and the GGA+ $U$ , respectively, which are similar to experimental value of  $2.2 \mu_B/\text{Cr}$ .<sup>4</sup>

Figure 2 presents the phonon dispersion curves and the phonon partial density of states (DOS) of  $\text{K}_2\text{Cr}_8\text{O}_{16}$  in its FM phase. Figure 2(a) and (b) were calculated without and with  $U$ , respectively. In both cases, flat bands are observed at  $\sim 10$  meV, which correspond to the localized phonon bands from K. The significant difference between phonon bands of the GGA and the GGA+ $U$  is the existence of the phonon softening instability in the latter (Fig.2(b)), which indicates the structural instability of the FM phase of  $\text{K}_2\text{Cr}_8\text{O}_{16}$  in agreement with the experiment. The fact that the phonon softening instability is obtained in the GGA+ $U$  but not in the GGA reflects that the GGA+ $U$  phonon calculation describes the experimental structural transition properly, while the GGA phonon calculation does not. It is seen that softened phonon modes are mostly from Cr and corner-shared O(2), and the softening instabilities are strong at M, X, and  $\Gamma$ .

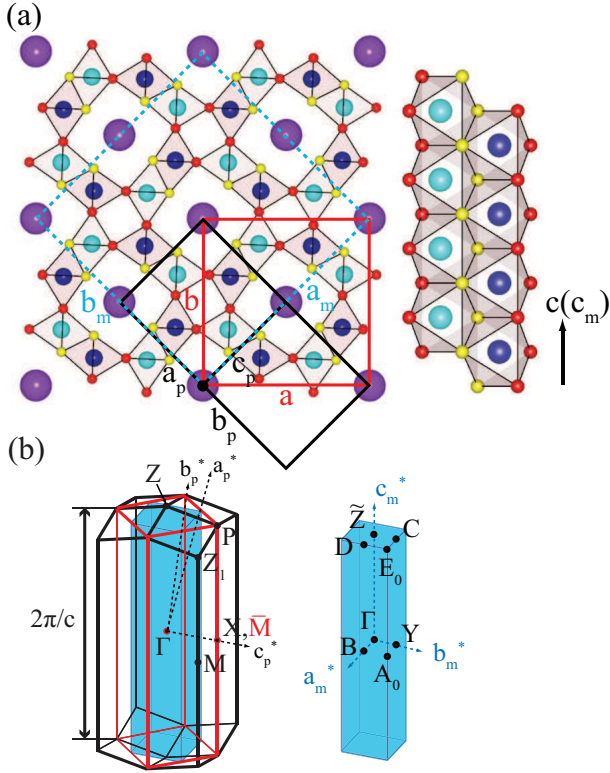


FIG. 1: (Color online) (a) Crystal structure of  $\text{K}_2\text{Cr}_8\text{O}_{16}$ . Black and red lines represent the primitive and the conventional unit cell of the FM phase, respectively, while dotted blue represents the unit cell of the FI phase. Purple, blue, sky-blue, yellow, and red balls represent K, Cr( $z=0$ ), Cr( $z=0.5$ ) O(1), and O(2), respectively. Right is the double-chain of edge-shared  $\text{CrO}_6$  octahedra along the  $c$  axis. In the FM phase, there are two types of O sites, edge-shared O(1) and corner-shared O(2). (b) Brillouin zone of  $\text{K}_2\text{Cr}_8\text{O}_{16}$ . Black and red lines represent the BZ's of the primitive and the conventional cell of the FM phase, respectively, and the blue filled box represents the BZ of the FI phase.  $(a_p^*, b_p^*, c_p^*)$  and  $(a_m^*, b_m^*, c_m^*)$  are reciprocal lattice vectors of the primitive body-centered tetragonal unit cell of the FM phase and the monoclinic unit cell of the FI phase, respectively. Note that, in the FM phase,  $\bar{M}$  of the BZ of the conventional cell is equivalent to X of the BZ of the primitive cell.

To investigate the phonon softenings in more detail, let us examine the low temperature structure of FI phase of  $\text{K}_2\text{Cr}_8\text{O}_{16}$ . The main difference between the FM phase and the FI phase is the increased unit cell size by  $\sqrt{2} \times \sqrt{2} \times 1$  with respect to the conventional cell of the FM phase due to the distortions of Cr and O. Toriyama *et al.*<sup>2</sup> reported that, on the  $ab$  plane, there is a stripe-type arrangement of the Cr tetramers formed in the four-chain columns. To explain the modulation of the tetragonal cell in the  $a$  and  $b$  directions, there should be a  $\bar{M}$  point softening in the conventional tetragonal cell, which actually corresponds to the X point in the primitive cell of the FM phase. Note that this  $\mathbf{Q}(\equiv \mathbf{X})$  vector is different from the previously suggested Peierls nesting vector  $\mathbf{Q}_z = 2\pi/c$ ,<sup>2</sup> which actually corresponds to M point  $(1/2, 1/2, -1/2)$  in the primitive cell or  $\Gamma$  point in the conventional cell.

Figure 3 shows the lattice displacements of softened phonon modes at X and M. The X softening in Fig. 3(a) and (b) produces not only the formation of Cr tetramer in the four-chain column along the  $c$  direction but also the stripe-type arrangement of Cr tetramers on the  $ab$  plane,

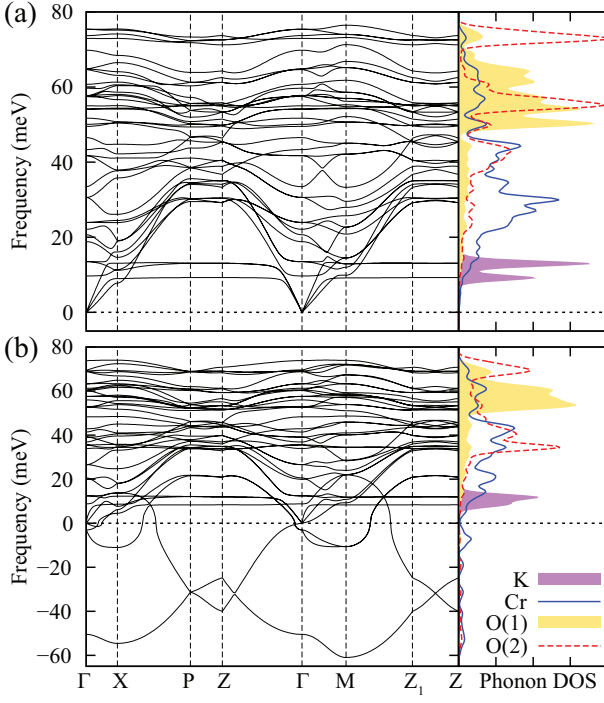


FIG. 2: (Color online) Phonon dispersion curves and the corresponding partial DOSs of  $\text{K}_2\text{Cr}_8\text{O}_{16}$  in its FM phase : (a) result from the GGA, and (b) result from the GGA+ $U$ . The k-point symmetry lines are along the BZ boundaries of primitive unit cell of the FM phase. The negative phonon frequencies (imaginary frequencies) reflects the phonon softening instability.

as shown in Fig.4(a). The formation of Cr tetramers shown in Fig.3(b) is perfectly consistent with that reported by Toriyama *et al.*<sup>2</sup> The stripe-type arrangement of Cr tetramers explains the unit cell increasing on the  $ab$  plane after the MIT. Namely, the normal modes of softened phonon at X is exactly consistent with the experimental lattice distortions.

Figure 3(c) and (d) present the lattice displacements by the softened phonon at M, which is the previously suggested Peierls nesting vector,  $Q_z = 2\pi/c$ .<sup>2</sup> The formation of Cr tetramers is also obtained in this case, as shown in Fig.3(d). However, the arrangement of Cr tetramers on the  $ab$  plane is different from the experimentally observed stripe-type. In this case, the arrangement is of uniform-type, as shown in Fig.4(b), which can not explain the increasing unit cell from the FM phase to the FI phase. This results is somehow expected because M point in the primitive cell of the FM phase is the same position as  $\Gamma$  point in the conventional tetragonal cell of the FM phase. That is why the M point softening produces the uniform-type arrangement of Cr tetramers, which does not increase the unit cell in the  $ab$  plane. We thus suggest that the nesting vector  $\mathbf{Q}$  that yields the Peierls instability is X (0, 0, 1/2) in the primitive cell of the body-centered tetragonal structure, not M (1/2, 1/2, -1/2).

The main difference between the lattice displacements of softened phonons at X and M lies in the linking of Cr-Cr in the double-chains of the edge-shared  $\text{CrO}_6$  octahedra. If Cr atoms in each chain move oppositely, the Cr-Cr dimerization of zig-zag type is formed in the double-chain, as shown in Fig. 3(d). Otherwise, there is no Cr-Cr dimerization (Fig. 3(b)). Due to these two possibilities of Cr-Cr linkings in the double-chains, there occur three types of arrangements of Cr tetramers,<sup>15</sup> as shown in Fig. 4. The stripe-type in Fig. 4(a) contains the half of double-chains with Cr dimers, while the uniform-type in Fig. 4(b) and the checkerboard-type in Fig. 4(c) have all and none of the double-chains with Cr dimers, respectively. Noteworthy is that these three types of arrangements match exactly with the normal mode displacements of softened phonons at X, M and  $\Gamma$ .

To check the role of the Cr-Cr dimers in the double-chains, we calculated the electronic structures of the above three modulated structures. Intriguingly, the insulating phases are obtained for all three cases, regardless of the existence of the Cr-Cr dimers in the double-chain.

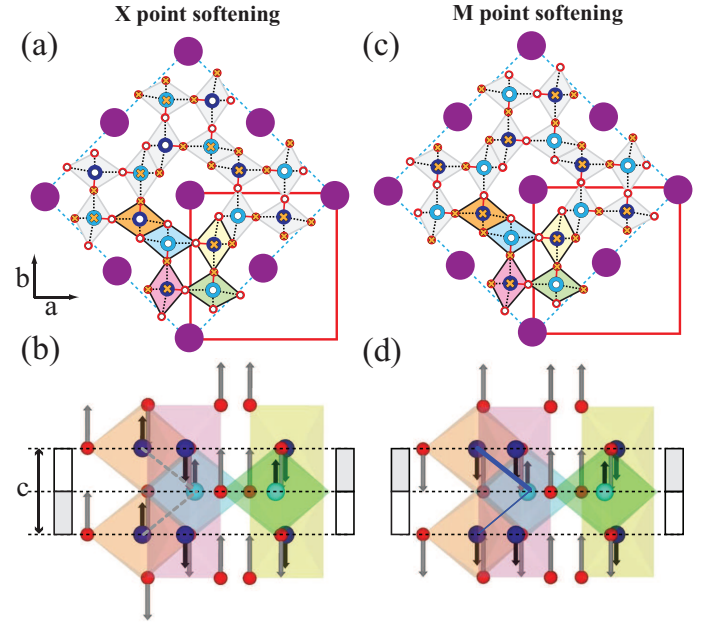


FIG. 3: (Color online) (a),(b) Lattice displacements of the softened phonon mode at X, and (c),(d) those at M. Purple, blue, sky-blue, and red circles are K, Cr( $z=0$ ), Cr( $z=0.5$ ) and O respectively. White circles and orange crosses at Cr and O in (a) and (c) denote the outward and inward arrows, respectively. (b) and (d) show the main atomic displacements of Cr and O(2), which lead to the formation of Cr tetramers. Gray and white boxes are shorter (corresponding to a tetramer) and longer parts of the four-chain columns. Dotted gray lines connecting Cr ions in (b) stand for the uniform distance between Cr-Cr in the double-chains, whereas thick and thin blue lines in (d) for the shorter and longer distances between Cr-Cr in the double-chains, respectively.

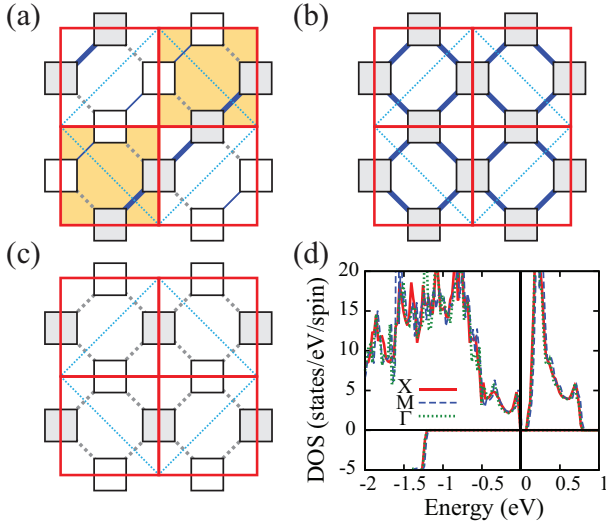


FIG. 4: (Color online) The arrangements of Cr tetramers on the  $ab$  plane obtained from the phonon softening mode. (a) the stripe-type arrangement by the phonon softening at X. Yellow shadow indicates the modulation of the tetragonal structure of the FM phase in the  $ab$  plane. (b) the uniform-type arrangement by the phonon softening at M. (c) the checkerboard-type arrangement by the phonon softening at  $\Gamma$ . Dotted gray, thick and thin blue lines connecting Cr ions in the double-chains are the same as in Fig. 3. (d) Total DOS of each arrangement obtained in the GGA+ $U$ .

The energy gap is  $\sim 0.1$  eV for all three cases, which is similar to the energy gap of the FI phase.<sup>2</sup> This result indicates that the insulating nature of the FI phase originates from the formation of Cr tetramers in the four-chain columns, not from the Cr-Cr dimers in the double-chains.

We also checked the roles of the Coulomb correlation  $U$  and the Peierls dimerization in the MIT and the structural transition. To investigate the  $U$  effect in the FM phase, the charge density difference (CDD) between the GGA+ $U$  and GGA calculations is plotted in Fig. 5(a). It is seen that Cr  $d_{yz+zx}$  and O(2)  $p_z$  electrons are more occupied in the GGA+ $U$  than in the GGA, while Cr  $d_{yz-xz}$  electrons are less occupied. This feature suggests that the hybridization between Cr  $d_{yz+zx}$  and O  $p_z$  orbitals increases with  $U$ . In fact, the Cr  $d_{yz+zx}$ -O  $p_z$  charge transfer path in the FI phase is emphasized in the recent NMR paper.<sup>19</sup> Therefore,  $U$  effect seems to facilitate the transition from the FM phase to the FI phase by increasing the hybridization between Cr  $d_{yz+zx}$  and O(2)  $p_z$ . Phonon data and the CDD result are reminiscent of the correlation assisted Peierls transition or Mott-Peierls transition in  $\text{VO}_2$ .<sup>20-22</sup> But the unique feature of  $\text{K}_2\text{Cr}_8\text{O}_{16}$  is that the Mott-Peierls transition occurs in the fully spin-polarized band.

Figure 5(b) shows the role of  $U$  in the FI phase in the band gap opening. The band gap opens only when both the distortion and the Coulomb correlation are taken into account. Namely, the GGA calculation does not open the band gap, even in the presence of the Peierls dimerization. This implies that  $\text{K}_2\text{Cr}_8\text{O}_{16}$  belongs to a Mott-insulator. The band gap in the GGA+ $U$  is 0.125 eV, which is in agreement with the previous calculation.<sup>2</sup>

Figure 5(c) and (d) show GGA+ $U$  band structures of the FM and FI phases of  $\text{K}_2\text{Cr}_8\text{O}_{16}$ , calculated in the FI phase symmetry. In the band structure of the FM phase in Fig. 5(c), there is no band gap opening because of the absence of the Peierls distortion. That is, the band gap opens only in the presence of the Peierls distortion (Fig. 5(d)). Through the lattice distortion, the energy gain is obtained mainly from bands at  $\tilde{Z}$ ,  $E_0$ , and A, which are in BZ boundary along the  $c^*$  direction (see Fig. 1(b)). The energy gain from the lattice dimerization in this case is  $\sim 19$  meV/f.u..

In conclusion, based on the systematic studies of electronic and phonon properties, we have found that  $\text{K}_2\text{Cr}_8\text{O}_{16}$  is a strongly correlated system having the Coulomb correlation effect both in the FM and the FI phases. We demonstrated that the phonon softening instability that occurs at X only in the GGA+ $U$  scheme describes perfectly well the experimentally observed lattice distortions, such as the formation of Cr tetramers along the  $c$  direction and the stripe-type arrangement of

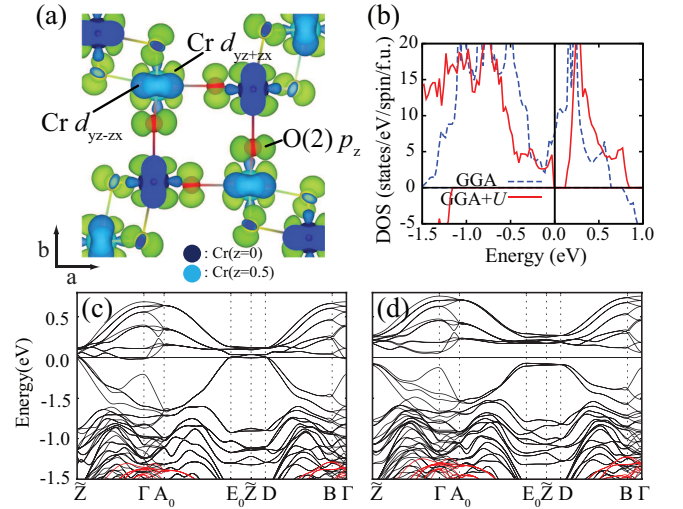


FIG. 5: (Color online) (a) The CDD between the GGA+ $U$  and the GGA for the FM phase of  $\text{K}_2\text{Cr}_8\text{O}_{16}$ . Green and blue represent the positive and negative part, respectively. The Cr tetramer, indicated by the red line, is seen to be connected by the  $\pi$ -bonding. (b) Comparison of total DOSs of the GGA and the GGA+ $U$  for the FI phase of  $\text{K}_2\text{Cr}_8\text{O}_{16}$ . GGA+ $U$  band structure of (c) the FM phase with the FI phase symmetry (c) The GGA+ $U$  band structure of the FM phase of  $\text{K}_2\text{Cr}_8\text{O}_{16}$  and (d) that of the FI phase of  $\text{K}_2\text{Cr}_8\text{O}_{16}$ , both of which are plotted in the BZ of the FI phase. Spin-majority and minority bands are plotted by black and red lines, respectively.

Cr tetramers on the  $ab$  plane. Due to the Coulomb correlation effect in the FM phase, the orbital redistribution from  $\text{Cr}d_{yz-zx}$  to  $\text{Cr}d_{yz+zx}$ - $\text{O}(2)p_z$  occurs, which facilitates the phase transition from the FM phase to the FI phase. Thus we proposed the correlation-assisted Peierls-like transition as the mechanism of the concomitant MIT and the structure transition in  $\text{K}_2\text{Cr}_8\text{O}_{16}$ . Our finding of softening vector  $\mathbf{Q}=\mathbf{X}$  rules out the previously suggested nesting vector of  $\mathbf{Q}_z=2\pi/c$  for the Peierls-like transition in  $\text{K}_2\text{Cr}_8\text{O}_{16}$ . We also showed that both the lattice dis-

placements and the Coulomb correlation effect are essential in opening the insulating gap of the FI phase, which indicates that the FI phase of  $\text{K}_2\text{Cr}_8\text{O}_{16}$  is a Mott-Peierls insulator.

**Acknowledgments**— This work was supported by the NRF (No. 2009-0079947, No. 2011-0025237), and the KISTI supercomputing center (No. KSC-2012-C2-094). S.K. acknowledges the support from the NRF project of Global Ph.D. Fellowship (No. 2011-0002351).

- 
- <sup>1</sup> M. Imada, A. Fujimori, and Y. Tokura, *Rev. Mod. Phys.* **70**, 1039 (1998).
  - <sup>2</sup> T. Toriyama, A. Nakao, Y. Yamaki, H. Nakao, Y. Murakami, K. Hasegawa, M. Isobe, Y. Ueda, A. V Ushakov, D.I. Khomskii, S. V Streltsov, T. Konishi, and Y. Ohta, *Phys. Rev. Lett.* **107**, 266402 (2011).
  - <sup>3</sup> M. Isobe, S. Koishi, N. Kouno, J.-I. Yamaura, T. Yamauchi, H. Ueda, H. Gotou, T. Yagi, and Y. Ueda, *J. Phys. Soc. Jpn.* **75**, 073801 (2006).
  - <sup>4</sup> K. Hasegawa, M. Isobe, T. Yamauchi, H. Ueda, J.-I. Yamaura, H. Gotou, T. Yagi, H. Sato, and Y. Ueda, *Phys. Rev. Lett.* **103**, 146403 (2009).
  - <sup>5</sup> K. Noami, Y. Muraoka, T. Wakita, M. Hirai, Y. Kato, T. Muro, Y. Tamenori, and T. Yokoya, *J. Appl. Phys.* **107**, 073910 (2010).
  - <sup>6</sup> M. Isobe, S. Koishi, S. Yamazaki, J. Yamaura, H. Gotou, T. Yagi, and Y. Ueda, *J. Phys. Soc. Jpn.* **78**, 114713 (2009).
  - <sup>7</sup> S. Horiuchi, T. Shirakawa, and Y. Ohta, *Phys. Rev. B* **77**, 155120 (2008).
  - <sup>8</sup> T. Toriyama, M. Watanabe, T. Konishi, and Y. Ohta, *Phys. Rev. B* **83**, 195101 (2011).
  - <sup>9</sup> O. Tamada, N. Yamamoto, T. Mori, and T. Endo, *J. Solid State Chem.* **126**, 1 (1996).
  - <sup>10</sup> M. Sakamaki, T. Konishi, and Y. Ohta, *Phys. Rev. B* **80**, 024416 (2009); *ibid.* **82**, 099903(E) (2010).
  - <sup>11</sup> M. A. Korotin, V. I. Anisimov, D. I. Khomskii, and G. A. Sawatzky, *Phys. Rev. Lett.* **80**, 4305 (1998).
  - <sup>12</sup> D.I. Khomskii and G.A. Sawatzky, *Solid State Commun.* **102**, 87 (1997).
  - <sup>13</sup> S. Nishimoto and Y. Ohta, *Phys. Rev. Lett.* **109**, 076401 (2012).
  - <sup>14</sup> P. Mahadevan, A. Kumar, D. Choudhury, and D.D. Sarma, *Phys. Rev. Lett.* **104**, 256401 (2010).
  - <sup>15</sup> A. Nakao, Y. Yamaki, H. Nakao, Y. Murakami, K. Hasegawa, M. Isobe, and Y. Ueda, *J. Phys. Soc. Jap.* **81**, 054710 (2012).
  - <sup>16</sup> G. Kresse and J. Furthmüller, *Phys. Rev. B* **54**, 11169 (1996); *Comput. Mater. Sci.* **6**, 15 (1996).
  - <sup>17</sup> A. Togo, F. Oba, and I. Tanaka, *Phys. Rev. B* **78**, 134106 (2008).
  - <sup>18</sup> K. Parlinski, Z. Q. Li, and Y. Kawazoe, *Phys. Rev. Lett.* **78**, 4063 (1997).
  - <sup>19</sup> H. Takeda, Y. Shimizu, M. Itoh, M. Isobe, and Y. Ueda, *Phys. Rev. B* **88**, 165107 (2013).
  - <sup>20</sup> S. Biermann, A. Poteryaev, A. I. Lichtenstein, and A. Georges, *Phys. Rev. Lett.* **94**, 026404 (2005).
  - <sup>21</sup> M. W. Haverkort, Z. Hu, A. Tanaka, W. Reichelt, S. V. Streltsov, M. A. Korotin, V. I. Anisimov, H. H. Hsieh, H.-J. Lin, C. T. Chen, D. I. Khomskii, and L. H. Tjeng, *Phys. Rev. Lett.* **95**, 196404 (2005).
  - <sup>22</sup> S. Kim, K. Kim, C.-J. Kang, and B.I. Min, *Phys. Rev. B* **87**, 195106 (2013).